

## Flux pinning mechanisms in $\text{ErNi}_2\text{B}_2\text{C}$

S. S. James,<sup>1</sup> C. D. Dewhurst,<sup>2</sup> S. B. Field,<sup>3</sup> D. McK. Paul,<sup>4</sup> Y. Paltiel,<sup>5</sup> H. Shtrikman,<sup>5</sup> E. Zeldov,<sup>5</sup> and A. M. Campbell<sup>1</sup>

<sup>1</sup>*Interdisciplinary Research Centre in Superconductivity, Madingley Road, Cambridge CB3 0HE, United Kingdom*

<sup>2</sup>*Institut Laue Langevin, BP156-38042, Grenoble, France*

<sup>3</sup>*Department of Physics, Colorado State University, Fort Collins, Colorado 80523-1875*

<sup>4</sup>*Department of Physics, University of Warwick, Coventry CV4 7AL, United Kingdom*

<sup>5</sup>*Department of Condensed Matter Physics, The Weizmann Institute of Science, 76100 Rehovot, Israel*

(Received 18 April 2001; published 15 August 2001)

We present local Hall probe measurements of the superconducting and magnetically ordered material  $\text{ErNi}_2\text{B}_2\text{C}$  ( $T_c \approx 10.5$  K,  $T_N \approx 6$  K). The onset of incommensurate antiferromagnetic order at  $T_N$ , within the superconducting state, results in an increase in vortex pinning for  $\mathbf{B} \parallel c$ . For  $\mathbf{B} \perp c$  no increase in pinning is observed at  $T_N$ , consistent with the notion of vortex pinning by planar magnetic domain boundaries for  $\mathbf{B} \parallel c$ . The development of a weak ferromagnetic component below  $T_{wf} \approx 2.5$  K results in a further increase in pinning for both orientations, suggesting that a different mechanism is responsible for this second increase at lower temperatures.

DOI: 10.1103/PhysRevB.64.092512

PACS number(s): 74.25.Dw, 74.25.Ha, 74.60.Ge, 74.70.Dd

$\text{ErNi}_2\text{B}_2\text{C}$  is a fascinating material exhibiting both superconductivity and antiferromagnetic order below  $T_c \approx 10.5$  K and  $T_N \approx 6$  K respectively.<sup>1-3</sup> It is a member of the  $R\text{Ni}_2\text{B}_2\text{C}$  series of materials in which the rare earth (RE) can be occupied by one of the magnetic (Er, Tm, Ho, Dy, Pr, Nd, Tb, Gd) or nonmagnetic (Lu, Y) elements. The superconducting transition temperatures vary from about 15 K for  $R = \text{Lu}$  or  $\text{Y}$ , down to 6 K for  $R = \text{Dy}$ , where strong pair breaking by the magnetic RE moments leads to reduced values of  $T_c$ , scaling roughly with the de Gennes factor associated with the RE moment. Superconducting upper critical fields  $B_{c2}$  are as high as 10 T ( $R = \text{Lu}$ ) with the Ginzburg-Landau parameter  $\kappa$  around 5. Reviews of superconductivity and magnetic order in the  $R\text{Ni}_2\text{B}_2\text{C}$  materials are given in Refs. 2 and 3.

The magnetic ordering of the RE ion is in most cases an antiferromagnetic spin density wave (SDW), although the modulation vector occurs along various crystal directions for the different members of the series.<sup>3</sup> The SDW can be either commensurate with the crystal structure (Nd, Dy, Pr, Ho) or incommensurate (Er, Tm, Tb, Ho).<sup>3</sup> In  $\text{ErNi}_2\text{B}_2\text{C}$  the  $\text{Er}^{3+}$  moments order into an incommensurately modulated SDW (Ref. 4) at  $T_N$ . This is accompanied by an increasingly orthorhombic distortion<sup>5</sup> with decreasing temperature below  $T_N$  which causes twinned structural domains to form.<sup>6</sup> The  $\text{Er}^{3+}$  moments are modulated along the longer  $a$  axis with incommensurate wave vector  $(0.5536, 0, 0)$ .<sup>2-4</sup> This modulation “squares up” continuously with decreasing temperature as higher-order harmonics are introduced. The onset of  $a$ -axis incommensurate order is thought to be responsible for strong pair breaking and the suppression of  $B_{c2}$  close to the ordering temperature.<sup>2,7</sup> A weak ferromagnetic component develops below  $T_{wf} \approx 2.5$  K where the magnetic modulation is modified by the appearance of ferromagnetic domain walls with two aligned spins at intervals along the SDW.<sup>8</sup> These boundaries are correlated in the  $b$ - $c$  plane to form planar ferromagnetic sheets with adjacent sheets not well coupled to others along the  $a$  axis. The result of these domain walls (not

to be confused with the structural domain walls which appear below  $T_N$ ) is a net moment of about  $0.3 \mu_B/\text{Er}$  in the  $b$ -axis direction.<sup>4,9</sup>

Small-angle neutron scattering (SANS) measurements of the mixed state in the  $R\text{Ni}_2\text{B}_2\text{C}$  materials<sup>10-13</sup> typically show the existence of a distorted hexagonal vortex lattice aligned with the crystallographic  $[100]$  axis at low fields which undergoes a transformation to a square lattice aligned with the  $[110]$  axis at high fields.<sup>12,13</sup> A coupling of vortices to the magnetic order in  $\text{ErNi}_2\text{B}_2\text{C}$  has been inferred from SANS measurements which show a rotation of vortices away from the applied field direction and disordering due to increased pinning in the weakly ferromagnetic state below  $\approx 2.5$  K.<sup>10</sup> Our pinning studies on  $\text{ErNi}_2\text{B}_2\text{C}$  (Ref. 14) and  $\text{HoNi}_2\text{B}_2\text{C}$  (Ref. 15) have shown that the onset of significant bulk pinning is coincident with the appearance of the  $a$ -axis incommensurate antiferromagnetic order when  $\mathbf{B} \parallel c$ ; i.e., pinning “switches on” in the temperature region in which the  $a$ -axis incommensurate SDW exists ( $T < 6$  K for  $\text{ErNi}_2\text{B}_2\text{C}$ ,  $5$  K  $< T < 6$  K for  $\text{HoNi}_2\text{B}_2\text{C}$ ). In Refs. 14 and 15 we speculated that vortices may interact with local magnetic moments at structural domain boundaries in the ordered state and therefore introduce pinning. Recent magneto-optical measurements of our crystals<sup>6</sup> have indeed verified that locally ferromagnetic domain boundaries exist only for temperatures below  $T_N$  for  $\text{ErNi}_2\text{B}_2\text{C}$ . The additional pair breaking due to this local moment at the domain walls provides a more reasonable explanation for the observed pinning enhancement than does the intrinsic magnetic modulation of the  $\text{Er}^{3+}$  ions themselves, which occurs over length scales far smaller than the vortex diameter.

Flux pinning in the  $R\text{Ni}_2\text{B}_2\text{C}$  materials is generally rather weak and vortex behavior is instead dominated by surface<sup>16,17</sup> and geometrical barrier effects.<sup>16,18,19</sup> The use of local Hall probes allows us to separate the intrinsic pinning behavior from these geometry dependent barrier effects. In this paper we present local Hall probe array measurements of single-crystal  $\text{ErNi}_2\text{B}_2\text{C}$ . We show that there is no significant increase in pinning for vortices aligned perpendicular to the  $c$

axis below the incommensurate magnetic ordering temperature  $T_N$  in contrast to the case where vortices are aligned parallel with the  $c$  axis.<sup>14</sup> Our results provide further evidence to suggest that the increase in pinning at  $T_N$  for  $\mathbf{B}\parallel c$ , which is absent for  $\mathbf{B}\perp c$ , is due to interaction with correlated pinning structures and is consistent with the magneto-optical studies.<sup>6</sup> Below  $T_{wf}$  pinning is further increased for vortices aligned in either direction indicating that a different mechanism is responsible for the second increase in pinning below this temperature.

Single crystals of  $\text{ErNi}_2\text{B}_2\text{C}$  were grown using a high-temperature flux method.<sup>1,20</sup> Crystals typically grow as small platelets with the  $c$  axis perpendicular to the platelet surface and are often optically smooth and therefore ideal for local Hall probe measurements. Samples were separated and cut into bars of around several hundred  $\mu\text{m}$  long by  $\approx 160 \mu\text{m}$  wide by  $\approx$  tens of  $\mu\text{m}$  thick using a fine wire saw. Sample edges were prepared in one of two ways. These were either natural crystal edges or were cut using a fine wire saw. The platelet surfaces were either the natural optically smooth surfaces or were polished until optically smooth using diamond-impregnated polishing paper (grit sizes down to  $0.5 \mu\text{m}$ ). The latter method was used to reduce the thickness of the as-grown platelets to achieve an optimal geometry for measurement or for measurements with the field aligned perpendicular to the  $c$  axis where optically smooth crystal surfaces do not readily occur in the natural growth. Linear arrays of Hall sensors were lithographically fabricated on GaAs wafers with an active GaAs/GaAlAs two-dimensional electron gas grown by molecular beam epitaxy.<sup>16</sup> Each of the 11 sensors has an active area of  $10 \mu\text{m}\times 10 \mu\text{m}$  and separation of  $10 \mu\text{m}$ . Samples were mounted face down onto the sensors using nonadecane wax with probes spanning the full width of the crystal.

Figure 1 shows field profile data for an  $\text{ErNi}_2\text{B}_2\text{C}$  crystal, prepared such that the  $c$  axis was perpendicular to the applied field ( $\mathbf{B}\perp c$ ). The crystal is one of the bar-shaped samples used in Ref. 14, turned on its side such that the applied field was now perpendicular to the  $c$  axis. Profiles are presented for both the increasing (open symbols) and decreasing (solid symbols) applied field sections of the hysteresis loop. At low fields, below the field for first penetration,  $B_{pen}$ , the probe responses in the region covered by the sample are Meissner shielded after initial zero-field cooling of the sample. A large gradient in the internal field close to the sample edges means that large shielding currents are present. This indicates that surface and geometrical barrier effects influence significantly the penetration and equilibrium and nonequilibrium distribution of vortices within the sample at all temperatures. Surface and geometrical barrier effects are discussed in detail in Refs. 16–19 and Refs. 14, 15, and 21 in relation to the  $\text{RNi}_2\text{B}_2\text{C}$  materials.

Figure 1(a) shows field profiles at 7.0 K. As expected above  $T_N$ , a single-dome profile on increasing field and almost flat profile on decreasing field indicate that bulk pinning is weak and the vortex response is dominated by surface and geometrical barriers.<sup>14,21</sup> A similar behavior is shown in Fig. 1(b) at 4.8 K, below the magnetic ordering temperature. The field profiles are again dome like and are very similar to

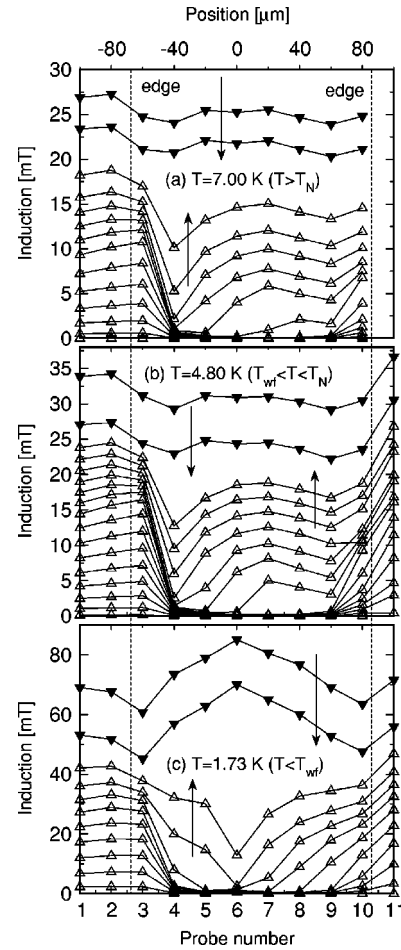


FIG. 1. Field profiles for  $\text{ErNi}_2\text{B}_2\text{C}$  with  $\mathbf{B}\perp c$  at (a) 7.0 K ( $T > T_N$ ), (b) 4.8 K ( $T_{wf} < T < T_N$ ), and (c) 1.73 K ( $T < T_{wf}$ ), for increasing (open symbols) and decreasing (solid symbols) applied field.

those recorded above  $T_N$  [Fig. 1(a)] in clear contrast to the behavior observed for  $\mathbf{B}\parallel c$  where bulk pinning “switches on” rather abruptly with the onset of magnetic order.<sup>14,15</sup> This indicates that the pinning centers introduced by the magnetic order appear to be ineffective for this field orientation at 4.8 K.

Figure 1(c) shows field profiles at 1.73 K, i.e., below  $T_{wf}$  where a ferromagnetic component of the magnetic order develops. The field profiles in Fig. 1(c) are very different from those in Figs. 1(a) and 1(b) and exhibit a distinct ‘V’ shape towards the sample center in increasing field and ‘inverted-V’ shape in decreasing field. This is characteristic of significant bulk pinning and a critical state. The effects of strong surface and geometrical barriers continue to modify the shape of the internal field profiles in ascending applied field where the profiles are more rounded close to the sample edges. The double-dome profile shown in Fig. 1(c) is typical of that observed when surface and geometrical barriers operate in combination with bulk pinning. Thus, for  $\mathbf{B}\perp c$ , significant bulk pinning only appears to be effective below  $T_{wf} \approx 2.5$  K.

To carefully distinguish between regions where bulk pinning is significant or where edge barriers dominate, the in-

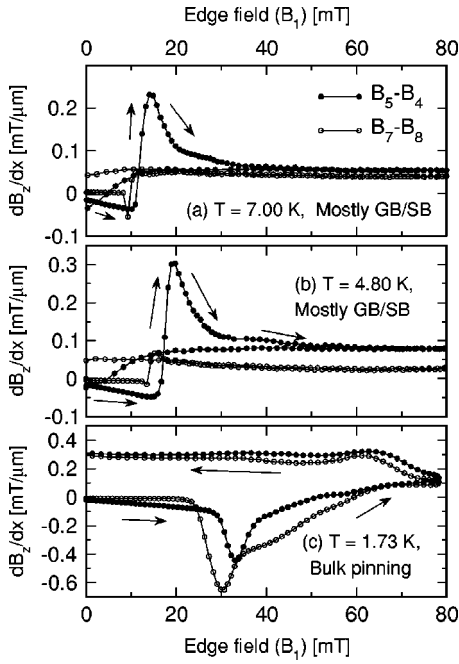


FIG. 2. Field gradient  $\partial B_z / \partial x$ , vs edge field  $\mathbf{B}_1$  at (a) 7.00 K, (b) 4.80 K, and (c) 1.73 K corresponding the flux profiles presented in Fig. 1.  $\partial B_z / \partial x$  is approximated by  $[B_5 - B_4]$  (solid symbols) and  $[B_7 - B_8]$  (open symbols), divided by their spatial separation.

ternal field gradient  $\partial B_z / \partial x$  can be analyzed as a function of field or temperature. We approximate  $\partial B_z / \partial x$  as the difference in induction between adjacent pairs of probes, divided by their spatial separation.<sup>16</sup> Figure 2 shows the field gradient plotted against the edge field,  $\partial B_z / \partial x$  vs  $B_1$ , for data presented in Fig. 1 at temperatures of 7.00 K ( $T > T_N$ ), 4.80 K ( $T_{wf} < T < T_N$ ), and 1.73 K ( $T < T_{wf}$ ). In each figure  $\partial B_z / \partial x$  is plotted for two pairs of probes,  $[B_5 - B_4]$  (solid circles) and  $[B_7 - B_8]$  (open circles). Determination of the internal field gradients from several pairs of sensors on opposite sides of the crystal provides a useful consistency check and is particularly important when there are significant asymmetries in the strengths of the surface barriers.<sup>14</sup> Figures 2(a) and 2(b) show  $\partial B_z / \partial x$  vs  $B_1$  at 7.00 K and 4.80 K, respectively, when surface and geometrical barriers dominate the hysteretic response and bulk pinning is almost entirely absent. The domelike profile in increasing field results in a positive  $\partial B_z / \partial x$  while an almost flat profile in decreasing field results in value close to zero and consequently a ‘‘clockwise’’  $\partial B_z / \partial x$  hysteresis loop. Figure 2(c) shows that when bulk pinning dominates,  $\partial B_z / \partial x$  traces an ‘anticlockwise’ loop and is more symmetric due to the V- and inverted-V-shaped profiles for increasing and decreasing fields. The magnitude of the field gradient close to the sample center allows an estimate for the critical current density to be made and is of the order of  $10^5$  A  $\text{cm}^{-2}$  at 1.73 K, approximately an order of magnitude greater than for  $\mathbf{B} \parallel c$  at similar temperatures.

In Fig. 3 we plot  $\partial B_z / \partial x$  vs temperature (at fixed  $B_1$ ) for both orientations  $\mathbf{B} \parallel c$  and  $\mathbf{B} \perp c$  extracted from a number of field profile measurements at closely spaced temperature intervals. Data are presented for both increasing and decreasing

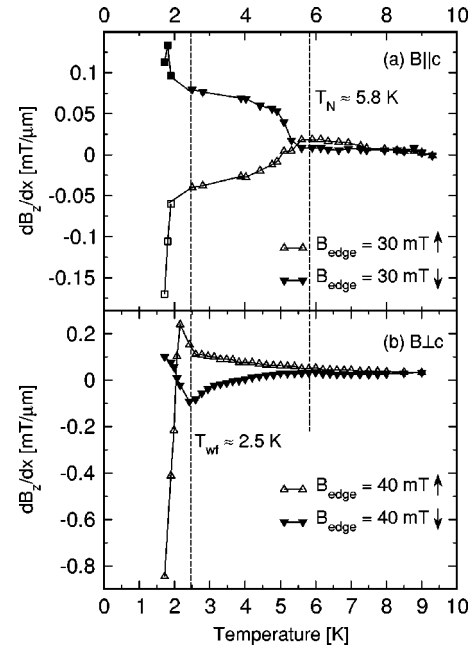


FIG. 3. Field gradient  $\partial B_z / \partial x$ , vs temperature for increasing (open symbols) and decreasing (closed symbols) field cycles at constant edge field,  $B_{edge}$ , for (a)  $\mathbf{B} \parallel c$  at 30 mT (triangles: Dewhurst *et al.*<sup>14</sup>; squares: this work) and (b)  $B_5 - B_6$  at 40 mT for  $\mathbf{B} \perp c$  (this work).

ing branches of the hysteresis loop. A negative (positive)  $\partial B_z / \partial x$  in increasing (decreasing) field indicates that bulk pinning dominates the vortex behavior while a positive (close to zero)  $\partial B_z / \partial x$  in increasing (decreasing) field is due to surface and geometrical barriers and the absence of bulk pinning. Figure 3(a) shows  $\partial B_z / \partial x$  vs temperature ( $B_1 = 30$  mT) for the  $\text{ErNi}_2\text{B}_2\text{C}$  crystal for which the applied field is parallel to the  $c$  axis, and includes data presented in Ref. 14. For  $\mathbf{B} \parallel c$  bulk pinning ‘‘switches on’’ at about 5.5 K from a background dominated by surface and geometrical barriers and almost coincident with the onset of magnetic order at  $T_N$ .<sup>14</sup> A further increase in the magnitude of  $\partial B_z / \partial x$  occurs at 2 K, just below  $T_{wf}$ . Figure 3(b), on the other hand, shows a very different behavior for  $\mathbf{B} \perp c$ . Surface and geometrical barriers dominate the vortex behavior continuously through  $T_N$ . A sharp change in gradient (and sign) of  $\partial B_z / \partial x$  at around  $T_{wf} \approx 2.5$  K shows that significant pinning switches on *only* below  $T_{wf}$ .

Recently, Saha *et al.*<sup>6</sup> have used magnetic decoration, magneto-optics, and scanning Hall probes to investigate vortices and magnetic domains in our  $\text{ErNi}_2\text{B}_2\text{C}$  single crystals. They show the existence of locally ferromagnetic planar domain boundaries along the  $[110]$  and  $[\bar{1}\bar{1}0]$  that appear only below  $T_N$  and are thought to accompany structural twin domains due to magnetoelectric distortion of the crystal lattice.<sup>5</sup> Saha *et al.* show that the domain boundaries have a ferromagnetic moment parallel to the domain plane direction ( $c$  axis) that is expected to lead to enhanced pair breaking at the domain walls. The spacing between domains is about 3–10  $\mu\text{m}$  and therefore may provide a suitable pinning microstructure for vortices below  $T_N$  for  $\mathbf{B} \parallel c$ . In a manner

analogous to heavily twinned  $\text{YBa}_2\text{Cu}_3\text{O}_{7-\delta}$ ,<sup>22,23</sup> “correlated” planar pinning centers yield a strong dependence of the pinning strength on the sample orientation and become largely ineffective when vortices are tilted away from the correlation direction. Our observation that pinning does not appear at  $T_N$  for  $\mathbf{B}\perp c$  supports strongly the notion that magnetic domain boundaries are responsible for the onset of pinning in  $\text{ErNi}_2\text{B}_2\text{C}$  below  $T_N$  with  $\mathbf{B}\parallel c$ .

Below  $T_{wf}$  a second increase in bulk pinning is observed for both orientations  $\mathbf{B}\parallel c$  and  $\mathbf{B}\perp c$  as reported by Gammel *et al.*<sup>8</sup> and shown here. The dramatic onset of pinning for  $\mathbf{B}\perp c$  below  $T_{wf}$  (well below  $T_c$ ) suggests that a different pinning mechanism is responsible below this temperature and that it is related to the onset of weak ferromagnetic order. Gammel *et al.* argue that the net ferromagnetic moment of  $0.3 \mu_B/\text{Er}$  can be interpreted as sharp domain walls in the SDW, i.e., ferromagnetically aligned spins every  $\approx 70 \text{ \AA}$ .<sup>8</sup> These local ferromagnetically coupled moments are also expected to cause enhanced pair breaking and therefore pinning for vortices. The spacing of the domain walls in the SDW ( $\approx 70 \text{ \AA}$ ) is far smaller than  $\lambda \approx 800 \text{ \AA}$ ,  $\xi \approx 150 \text{ \AA}$ , or the boundaries observed by Saha *et al.* and should be expected to exhibit pinning properties of a different nature from those

related to the twin domain boundaries of structural origin observed at higher temperatures.<sup>6</sup> The fact that we see increased pinning for both orientations below  $T_{wf}$ , but only for  $\mathbf{B}\parallel c$  below  $T_N$  provides strong evidence that the two magnetic-order-induced pinning mechanisms are different. These favoring a pointlike pinning description or correlated pinning in the former and latter case, respectively.

In summary, we have used local Hall probes to investigate vortex pinning in  $\text{ErNi}_2\text{B}_2\text{C}$  for  $\mathbf{B}\perp c$  and  $\mathbf{B}\parallel c$ . For vortices aligned perpendicular to the  $c$  axis, significant pinning develops only below  $T_{wf} \approx 2.5 \text{ K}$ , in contrast to  $\mathbf{B}\parallel c$  for which pinning “switches on” coincident with the  $a$ -axis incommensurate antiferromagnetic ordering transition at  $T_N \approx 5.8 \text{ K}$ . Demonstration of the pinning anisotropy below  $T_N$  provides further evidence that the magnetic-order-induced pinning for  $\mathbf{B}\parallel c$  is due to interaction with planar magnetic domain boundaries (correlated disorder) related to the tetragonal-to-orthorhombic structural transition. A different point disorder pinning mechanism is required to explain the second increase below  $\approx 2.5 \text{ K}$  observed for both crystalline orientations.

E.Z. acknowledges the support of the German-Israeli Foundation for Scientific Research and Development (GIF).

- 
- <sup>1</sup>B. K. Cho, P. C. Canfield, L. L. Miller, D. C. Johnston, W. P. Beyermann, and A. Yatskar, *Phys. Rev. B* **52**, 3684 (1995).
- <sup>2</sup>P. C. Canfield, P. L. Gammel, and D. J. Bishop, *Phys. Today* **51** (10), 40 (1998).
- <sup>3</sup>J. W. Lynn, S. Skanthakumar, Q. Huang, S. K. Sinha, Z. Hossain, L. C. Gupta, R. Magarajan, and C. Godart, *Phys. Rev. B* **55**, 6584 (1997).
- <sup>4</sup>S. K. Sinha, J. W. Lynn, T. E. Grigereit, Z. Hossain, L. C. Gupta, R. Nagarajan, and C. Godart, *Phys. Rev. B* **51**, 681 (1995).
- <sup>5</sup>C. Detlefs, D. L. Abernathy, G. Grübel, and P. C. Canfield, *Europhys. Lett.* **47**, 352 (1999).
- <sup>6</sup>N. Saha, R. Surdeanu, M. Marchevsky, G. J. Nieuwenhuys, C. D. Dewhurst, R. J. Wijngaarden, D. McK. Paul, and P. H. Kes, *Phys. Rev. B* **63**, 020502 (2001).
- <sup>7</sup>A. I. Goldman, C. Stassis, P. C. Canfield, J. Zarestky, P. Dervenagas, B. K. Cho, D. C. Johnston, and B. Sternlieb, *Phys. Rev. B* **50**, 9668 (1994).
- <sup>8</sup>P. L. Gammel, B. Barber, D. Lopez, A. P. Ramirez, and D. J. Bishop, *Phys. Rev. Lett.* **84**, 2497 (2000).
- <sup>9</sup>H. Kawano, H. Takeya, H. Yoshizawa, and K. Kadowaki, *J. Phys. Chem. Solids* **60**, 1053 (1999).
- <sup>10</sup>U. Yaron, P. L. Gammel, A. P. Ramirez, D. A. Huse, D. J. Bishop, A. I. Goldman, C. Stassis, P. C. Canfield, K. Mortensen, and M. R. Eskildsen, *Nature (London)* **382**, 236 (1996).
- <sup>11</sup>P. L. Gammel, D. J. Bishop, M. R. Eskildsen, K. Mortensen, N. H. Andersen, I. R. Fisher, K. O. Cheon, P. C. Canfield, and V. G. Kogan, *Phys. Rev. Lett.* **82**, 4082 (1999).
- <sup>12</sup>M. R. Eskildsen, P. L. Gammel, B. P. Barber, U. Yaron, A. P. Ramirez, D. A. Huse, D. J. Bishop, C. Bolle, C. M. Lieber, S. Oxx, S. Sridhar, N. H. Andersen, K. Mortensen, and P. C. Canfield, *Phys. Rev. Lett.* **78**, 1968 (1997).
- <sup>13</sup>D. McK. Paul, C. V. Tomy, C. M. Aegerter, R. Cubitt, S. H. Lloyd, E. M. Forgan, S. L. Lee, and M. Yethiraj, *Phys. Rev. Lett.* **80**, 1517 (1998).
- <sup>14</sup>C. D. Dewhurst, S. S. James, R. A. Doyle, Y. Paltiel, E. Zeldov, and D. McK. Paul, *Phys. Rev. B* **63**, 060501 (2001).
- <sup>15</sup>C. D. Dewhurst, R. A. Doyle, E. Zeldov, and D. McK. Paul, *Phys. Rev. Lett.* **82**, 827 (1999).
- <sup>16</sup>E. Zeldov, D. Majer, M. Konczykowski, A. I. Larkin, V. M. Vinokur, V. B. Geshkenbein, N. Chikumoto, and H. Shtrikman, *Europhys. Lett.* **30**, 367 (1995).
- <sup>17</sup>C. P. Bean and J. D. Livingston, *Phys. Rev. Lett.* **12**, 14 (1964).
- <sup>18</sup>E. Zeldov, A. I. Larkin, V. B. Geshkenbein, M. Konczykowski, D. Majer, B. Khaykovich, V. M. Vinokur, and H. Shtrikman, *Phys. Rev. Lett.* **73**, 1428 (1994).
- <sup>19</sup>E. H. Brandt, *Phys. Rev. B* **59**, 3369 (1999).
- <sup>20</sup>M. Xu, P. C. Canfield, J. E. Ostenson, D. K. Finnemore, B. K. Cho, Z. R. Wang, and D. C. Johnston, *Physica C* **227**, 321 (1994).
- <sup>21</sup>S. S. James, C. D. Dewhurst, R. A. Doyle, D. McK. Paul, E. Zeldov, and A. M. Campbell, *Physica C* **332**, 173 (2000).
- <sup>22</sup>I. Maggio-Aprile, C. Renner, A. Erb, E. Walter, and Ø. Fischer, *Nature (London)* **390**, 487 (1997).
- <sup>23</sup>B. Keimer, F. Doğan, I. A. Aksay, R. W. Erwin, J. W. Lynn, and M. Sarikaya, *Science* **262**, 83 (1993).